



OPEN

One-Step Instant Synthesis of Protein-Conjugated Quantum Dots at Room Temperature

Xuewen He, Li Gao & Nan Ma

The Key Lab of Health Chemistry and Molecular Diagnosis of Suzhou, College of Chemistry, Chemical Engineering and Materials Science Soochow University, Suzhou, 215123, P. R. China.

SUBJECT AREAS:

QUANTUM DOTS
CANCER IMAGING
NANOPARTICLES
ANALYTICAL CHEMISTRY

Received

15 August 2013

Accepted

12 September 2013

Published

2 October 2013

Correspondence and requests for materials should be addressed to N.M. (nan.ma@suda.edu.cn)

We present a new general facile strategy for the preparation of protein-functionalized QDs in a single step at ambient conditions. We demonstrated that highly luminescent red to near-infrared (NIR) protein-functionalized QDs could be synthesized at room temperature in one second through a one-pot reaction that proceeds in aqueous solution. Herein protein-functionalized QDs were successfully constructed for a variety of proteins with a wide range of molecular weights and isoelectric points. The as-prepared protein-conjugated QDs exhibited high quantum yield, high photostability and colloidal stability, and high functionalization efficiency. Importantly, the proteins attached to the QDs maintain their biological activities and are capable of catalyzing reactions and biotargeting. In particular, the as-prepared transferrin-QDs could be used to label cancer cells with high specificity. Moreover, we demonstrated that this synthetic strategy could be extended to prepare QDs functionalized with folic acids and peptides, which were also successfully applied to cancer cell imaging.

Quantum dots are superior luminophores with large extinction coefficient, strong photoluminescence, and robust photostability, which have proven to be powerful tools for bioimaging and biosensing^{1–12}. Proteins represent a central target in medical and biochemical research. Fluorescent labeling of proteins provides a useful means to explore the roles of proteins in fundamental biological processes and implement a variety of biomedical applications such as optical imaging and biosensing^{6,7,9,12,13}. However, preparation of protein-conjugated QDs is a laborious multi-step process that usually consists of colloidal QDs synthesis, QDs solubilization, and biomolecule functionalization^{4,5,7,8,14–16}. The stringent reaction conditions and synthetic complexities would prohibit the end-users from gaining direct access to customizable QD probes in an easy and efficient manner. So far direct aqueous synthesis of protein-conjugated QDs at ambient conditions has achieved little success in producing highly luminescent QDs that are competent for bioimaging applications^{17–19}.

In order to achieve one-step synthesis of protein-functionalized QDs, we developed a QD synthetic strategy that meets the following criteria: (i) the QDs should be enriched with certain metal ions that can coordinate with various amino acid functional groups (e.g. carboxyl group; amino group; thiol group, imidazole *et al.*), leading to effective binding of the protein with QD surface²⁰; (ii) the QDs synthesis reaction should proceed at ambient conditions (i.e. room temperature) rapidly to avoid protein denaturing; (iii) the as-prepared QDs should possess suitable emission range, high quantum yield (QY), and high photostability for bioimaging applications. Although DNA-functionalized CdTe QDs have been successfully constructed via a one-step strategy^{21,22}, the high temperature (100°C) and long reaction time (1 hour) required to synthesize CdTe QDs could not be applied to directly prepare protein-functionalized QDs since protein molecules would be easily denatured at high temperatures.

Results

In this study we report a new type of alloyed Zn_xHg_{1-x}Se QDs that fully meet the criteria for one-step synthesis of protein-functionalized QDs. The synthesis of Zn_xHg_{1-x}Se QDs is conducted in aqueous solution at room temperature and completed in one second, which surpasses the main obstacle for one-step preparation of protein-functionalized QDs. In particular, the as-prepared Zn_xHg_{1-x}Se QDs exhibiting strong red to NIR photoluminescence that is suitable for bioimaging, which can hardly be achieved for other types of QDs produced with the same synthetic strategy. Moreover, the Zn²⁺ ion could coordinate with a variety of amino acid residues (e.g. Asp/Glu (carboxyl group), His (imidazole), Tyr (hydroxyl group), Lys (amino group), and Cys (thiol group))^{23,24}, which would lead to effective binding of protein with zinc-based QDs. In this QD synthesis regime protein molecules



and small thiol-containing molecules (e.g. mercaptopropionic acid (MPA)) are both used as ligands simultaneously to generate protein-functionalized QDs (Figure 1). While protein molecules would bind to the QDs through the coordination of amino acid residues with Zn^{2+} ions on QD surface^{23,24}, the small thiol-containing MPA molecules would serve as additive QD ligands to achieve good surface passivation and optimal photoluminescence properties²². As a starting point, we first explore the synthesis of unfunctionalized $Zn_xHg_{1-x}Se$ QDs using MPA as ligands and $Zn(OAc)_2$, $Hg(ClO_4)_2$, and $NaHSe$ as precursors. In brief, $Zn(OAc)_2$, $Hg(ClO_4)_2$, and MPA are first mixed in NH_4HCO_3 solution (pH 12.3) after which $NaHSe$ is quickly injected into the mixture followed by vortexing (see experimental section for more details). The reaction mixture turned brown immediately after injecting $NaHSe$ (Figure 2), indicating instant formation of QDs. Different Hg/Zn precursor molar ratios (1%, 2%, 5%, 10%, 20%, 25%, 40%) were used for QD synthesis, as the Hg/Zn precursor ratio increases the absorption spectra and emission spectra of the as-prepared QDs both shifted to longer wavelength (SI section 1.1). The emission maximum shifted from 672 nm to 907 nm as the Hg/Zn precursor ratio increased from 1% to 40%. The QDs synthesized at Hg/Zn precursor ratio of 10% exhibit the highest quantum yield (QY = 25.6%) and an emission maximum at 704 nm (Table 1 and Figure 2). The size and morphology of the as-prepared QDs (Hg/Zn precursor ratio of 10%) were characterized using transmission electron microscopy (TEM). Near monodisperse spherical nanoparticles were obtained with a mean diameter of 4.0 ± 0.6 nm (Figure 2d). Lattice fringes can be clearly visualized in high-resolution TEM images, indicating the formation of nanocrystalline materials. STEM-EELS analysis confirms that the as-prepared $Zn_xHg_{1-x}Se$ QDs possess an alloy structure rather than a core-shell structure (SI section 2.1). The broad absorption spectrum of these $Zn_xHg_{1-x}Se$ QDs indicates that the QDs are inhomogeneous alloys²⁵. The elemental composition and the Zn/Hg/Se molar ratio in the as-prepared QDs were measured using inductively coupled plasma optical emission spectrometry (ICP-OES). The percentage of Hg incorporated into the QDs increases with elevated Hg/Zn precursor ratio (Table 1). The Zn/Hg/Se element molar ratio is 0.91 : 0.09 : 0.38 for the QDs synthesized at Hg/Zn precursor ratio of 10%. In order to obtain QDs with highest QY, in the following studies all the $Zn_xHg_{1-x}Se$ QDs were synthesized at Hg/Zn precursor ratio of 10%.

Next, we proceed to investigate one-step synthesis of protein-functionalized QDs based on the above synthetic strategy. We first selected bovine serum albumin (BSA) as a proof-of-concept study. BSA has a molecular weight (M.W.) of 66.4 kDa and an isoelectric point (pI) of 5.3. To synthesize BSA-functionalized $Zn_xHg_{1-x}Se$ QDs, BSA and MPA were used as co-ligands and the other reaction conditions were the same as unfunctionalized MPA-QDs. To explore the effects of protein concentration on QD functionalization efficiencies, five different BSA concentrations (0.25, 0.5, 1.0, 2.0, and 5.0 mg/mL) were tested for the syntheses. As shown in Figure 2a and 2b, there are slightly blue shifts of the absorption and emission spectra of BSA-QDs (5.0 mg/mL BSA) in comparison with unfunctionalized MPA-QDs. The photoluminescence intensity of BSA-QDs is almost same as MPA-QDs. The QY of BSA-QDs is 26.0%. These BSA-QDs have a mean diameter of 3.9 ± 0.5 nm and near spherical shape illustrated by TEM images (Figure 2d), which is quite analogous to MPA-QDs. QD functionalization with BSA was monitored using agarose gel electrophoresis since the photoluminescence of QDs can be directly detected. As shown in Figure 2e, the unfunctionalized QDs exhibit a single band with high mobility. The QDs synthesized with BSA exhibit an additional band with retarded mobility which is caused by the increased overall size of QDs after BSA functionalization. As the BSA concentration increases the luminescence intensity of the upper band increases while the luminescence intensity of the lower band decreases, indicating that a higher percentage of QDs can be functionalized with increasing BSA concentration. Most of QDs were

functionalized with BSA at a BSA concentration of 5.0 mg/mL. To further confirm the presence of BSA on the QDs, the agarose gel was stained with Coomassie brilliant blue. A series of blue bands can be visualized in the stained gel which completely co-localize with the upper QDs bands in the luminescence gel image, confirming the successful attachment of BSA to QDs (Figure 2e). Pure BSA-QD conjugates can be isolated and extracted from the agarose gel without affecting their integrality (SI section 4.2). Gel filtration chromatography (GFC) was also used to monitor QD functionalization in order to precisely measure the hydrodynamic (HD) size of the QDs and quantitate the fraction of protein-functionalized QDs. As shown in Figure 3, the unfunctionalized MPA-QDs exhibit a small hydrodynamic diameter of ~ 5.4 nm and a relatively narrow size distribution. The peak of BSA-QDs (5.0 mg/mL BSA) shifts to shorter elution time corresponding to a larger hydrodynamic diameter (~ 12.1 nm) as a result of the attachment of BSA to the QDs. The fraction of functionalized QDs is calculated to be 95%. The hydrodynamic diameters of MPA-QDs and BSA-QDs measured by dynamic light scattering (DLS) were 5.9 nm and 13.7 nm respectively, which are consistent with gel filtration chromatography results (SI section 2.5). The effects of QD on BSA structure were explored using circular dichroism (CD). Little changes were observed for the secondary structure of QD-associated BSA as compared to the native BSA (SI section 4.3). To explore whether the protein itself participates in the QD synthesis, we used BSA (5.0 mg/mL) as the only ligand to synthesize $Zn_xHg_{1-x}Se$ QDs. The QD formation with only BSA molecules is as efficient as that with both BSA and MPA molecules as revealed by the QD absorption spectra (SI section 1.2). In contrast, no QDs were produced in the absence of BSA and MPA molecules. TEM image further confirms the production of nanocrystalline QDs in the presence of only BSA molecules (SI section 2.2). These results suggest that BSA can indeed mediate the growth of QDs and attach to the QDs in a single step process. It is noteworthy that the photoluminescence intensity of the QDs produced with only BSA molecules is quite low due to insufficient surface passivation. The QD photoluminescence intensity can be drastically increased when MPA molecules are used as additive ligands for QD synthesis to improve QD surface passivation (SI section 1.2). The mechanism of BSA-mediated QD formation is explored by FTIR, UV-Vis spectroscopy, and TEM (SI section 6). The results show that the protein-directed QD synthesis undergoes the following mechanism: protein molecules first bind to metal ions to form a complex; this complex facilitates controlled nucleation following the introduction of anion precursors; the as-formed nuclei grow bigger to form QDs by reacting with the free precursors in solution; the protein passivates on QD surface once the QD is formed.

To further deconvolute the role of each type of amino acid residue in QD attachment, we performed selective chemical modification of each type of amino acid residue (amino group, thiol group, carboxyl group, imidazole group, hydroxyl group) in BSA in order to block their interaction with the QD respectively. Then we used each chemically modified BSA to synthesize QDs and quantitate the protein functionalization efficiency for the QDs to find out the contribution of each type of amino acid residue to protein attachment. Our results show that the carboxyl group, imidazole group, and hydroxyl group play an important role in protein attachment. Cysteine residues have almost no effect on protein attachment since most of cysteine residues form disulfide bonds in proteins (SI section 5). It is noteworthy that the occurrences of Asp/Glu (-COOH), His (imidazole), and Tyr (-OH) residues within BSA and a large protein population (105990 sequences) are at similar levels. Also, most of these hydrophobic residues are present on protein surface²⁶ and would be accessible for QD binding (SI section 5.4). Therefore, it is expectable that this QD synthetic strategy could be used for many other proteins.

To explore whether this QD synthetic strategy could serve as a general strategy to produce protein-functionalized QDs, we tested a

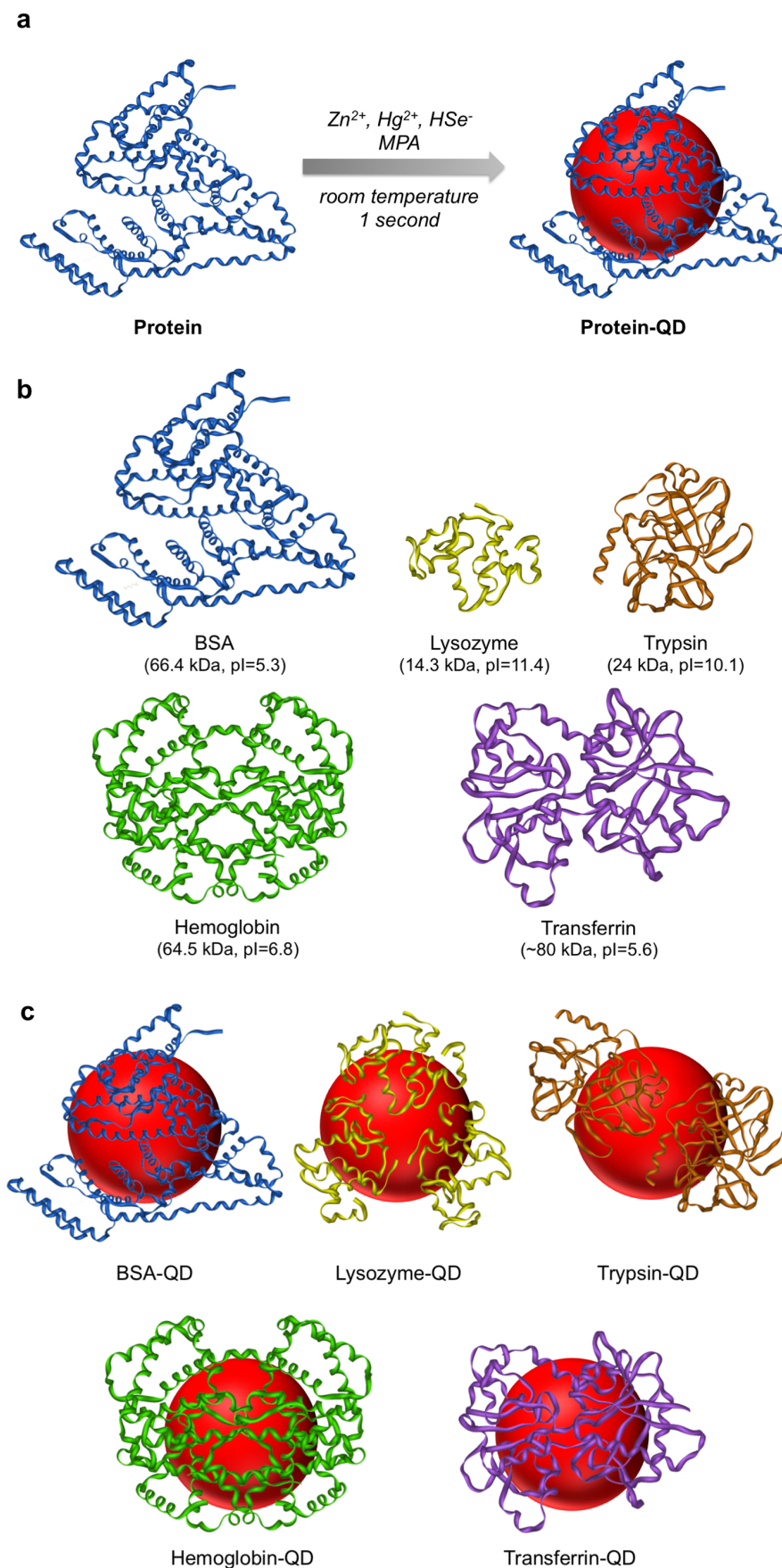


Figure 1 | Schematic illustration of one-step preparation of protein-functionalized QDs. (a) One-step synthesis of protein-functionalized $Zn_xHg_{1-x}Se$ QDs using Zn^{2+} , Hg^{2+} , and HSe^{-} ions as precursors and MPA and protein as co-ligands. The synthesis is conducted at room temperature and completed in one second. (b) Structures, molecular weights, and isoelectric points of BSA, lysozyme, trypsin, hemoglobin, and transferrin. (c) Schematic illustration of BSA-, lysozyme-, trypsin-, hemoglobin-, and transferrin-functionalized QDs.

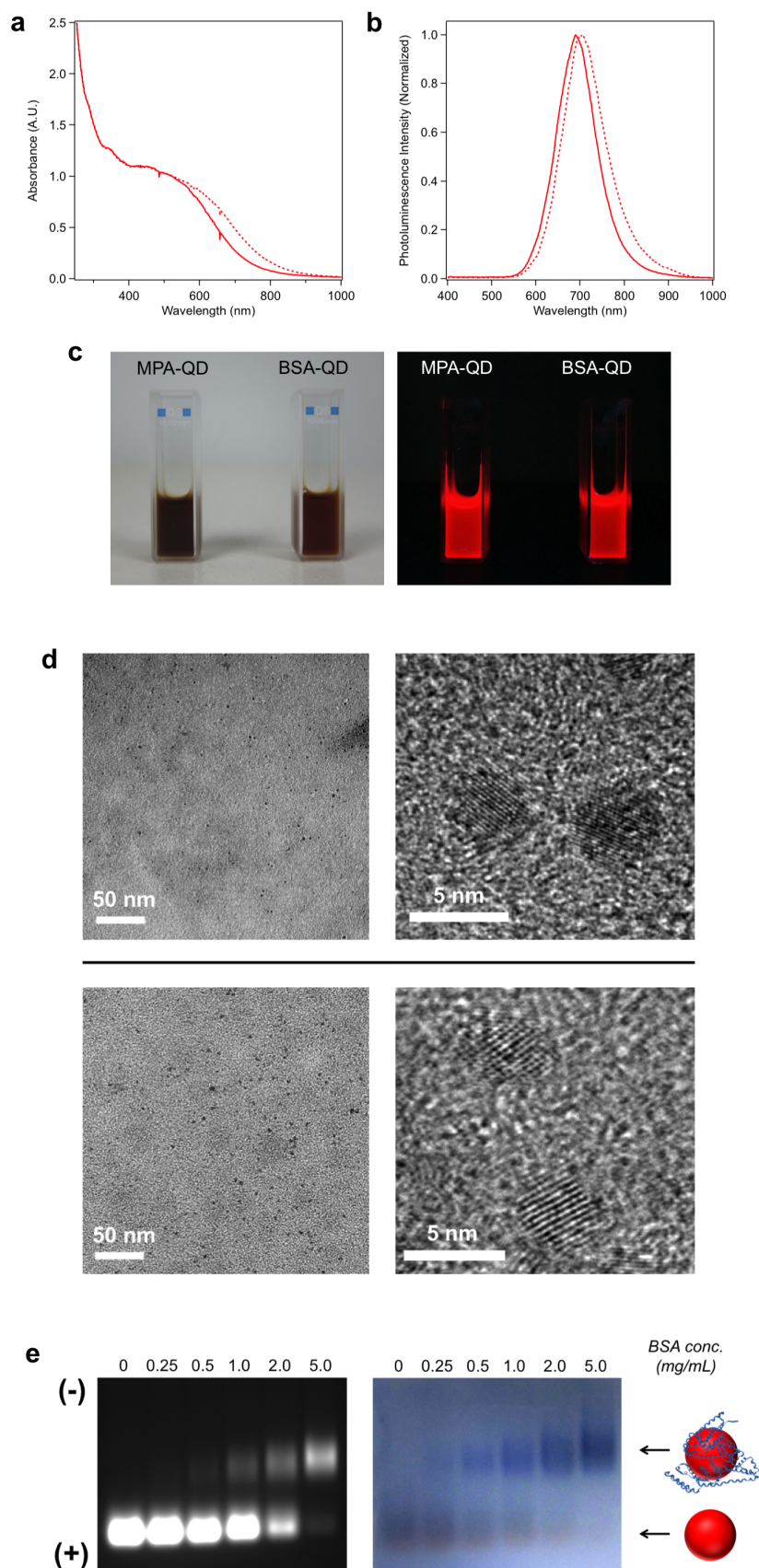


Figure 2 | Characterization of unfunctionalized MPA-QDs and BSA-functionalized QDs (5.0 mg/mL BSA). (a) Absorption spectra of MPA-QDs (dashed line) and BSA-QDs (solid line). (b) Photoluminescence spectra of MPA-QDs (dashed line) and BSA-QDs (solid line). (c) Photographs of MPA-QDs and BSA-QDs captured under visible light (left) and UV light (365 nm) (right). (d) Low magnification and high-resolution TEM images of MPA-QDs (upper panel) and BSA-QDs (lower panel). (e) Agarose gel electrophoresis of MPA-QDs and BSA-QDs synthesized at different BSA concentrations. The left gel image is the QD photoluminescence image. The right gel image is Coomassie brilliant blue-stained image showing the position of BSA (blue bands).



Table 1 | Elemental analysis, quantum yields, emission maxima, and FWHM of $Zn_xHg_{1-x}Se$ QDs synthesized at different Hg/Zn precursor molar ratios

	Hg/Zn precursor molar ratio	Hg/Zn molar ratio in QD	Zn/Hg/Se molar ratio in QD	QY	λ_{max} (nm)	FWHM (nm)
1	1%	4.2%	0.96:0.04:0.51	13.1%	672	166
2	2%	4.7%	0.95:0.05:0.50	16.4%	673	142
3	5%	8.5%	0.92:0.08:0.47	20.9%	684	126
4	10%	9.7%	0.91:0.09:0.38	25.6%	704	112
5	20%	18.0%	0.85:0.15:0.39	13.8%	736	141
6	25%	20.1%	0.83:0.17:0.35	4.3%	801	122
7	40%	26.9%	0.79:0.21:0.32	1.0%	907	151

variety of proteins with different molecular weights and isoelectric points including lysozyme (M.W. = 14.3 kDa, pI = 11.4), trypsin (M.W. = 24 kDa, pI = 10.1), hemoglobin (M.W. = 64.5 kDa, pI = 6.8), and transferrin (M.W. = 80 kDa, pI = 5.6). Protein-functionalized QDs were synthesized under the same conditions as BSA-QDs and were characterized using agarose gel electrophoresis (SI section 4.1). Similar to BSA-QDs, QDs synthesized with all the other proteins exhibited additional QD bands with retarded mobility in the agarose gel, implying successful functionalization of QDs with these proteins. At protein concentration of 5.0 mg/mL, the QDs synthesized with lysozyme, trypsin, and hemoglobin were almost completely functionalized while the QDs synthesized with transferrin were partially functionalized. Gel filtration chromatography was also used to monitor QDs functionalization. As shown in Figure 3, lysozyme-QD and trypsin-QD exhibited nearly entire peak shift to larger hydrodynamic sizes, indicating almost complete QD functionalization. Two separate peaks were observed for the QDs synthesized with transferrin, which correspond to the functionalized and unfunctionalized QDs respectively. The functionalization efficiency of transferrin-QD (5.0 mg/mL transferrin) is 47%. The attachment of hemoglobin to the QDs is validated by fluorescence resonance energy transfer (FRET). Hemoglobin is an iron-containing oxygen-transport

metalloprotein that exhibits strong absorption in the visible and near-IR region (SI section 4.4). Direct attachment of hemoglobin to the QD will result in efficient quenching of QD photoluminescence due to the small distance (<5 nm) between QD and hemoglobin. As shown in Figure 4a, with an increasing hemoglobin concentration for QD synthesis, a stepwise decrease of QD photoluminescence is observed. The quenching efficiency is 95.2% for the QDs synthesized with 5.0 mg/mL hemoglobin. To explore the impact of QDs on the biological activities of the protein, we measured the hydrolysis activities of lysozyme in native form and QD-associated form. Lysozyme activity is determined according to the lysis rate of *Micrococcus lysodeikticus* cells (see experimental section for more details). As shown in Figure 4b, 88% of hydrolysis activity is preserved for the QD-associated lysozyme, suggesting that the QD binding has marginal effects on lysozyme catalytic activity.

To explore the applicability of the as-prepared $Zn_xHg_{1-x}Se$ QDs for bioimaging, we first tested the photostability of these $Zn_xHg_{1-x}Se$ QDs and compared it with the traditional CdTe QDs. The QDs were continuously excited with a high power 405 nm laser (110 mW) and their photoluminescence spectra were recorded at different time points. After 60 min exposure to the 405 nm laser, both the unfunctionalized and BSA-functionalized $Zn_xHg_{1-x}Se$ QDs underwent a

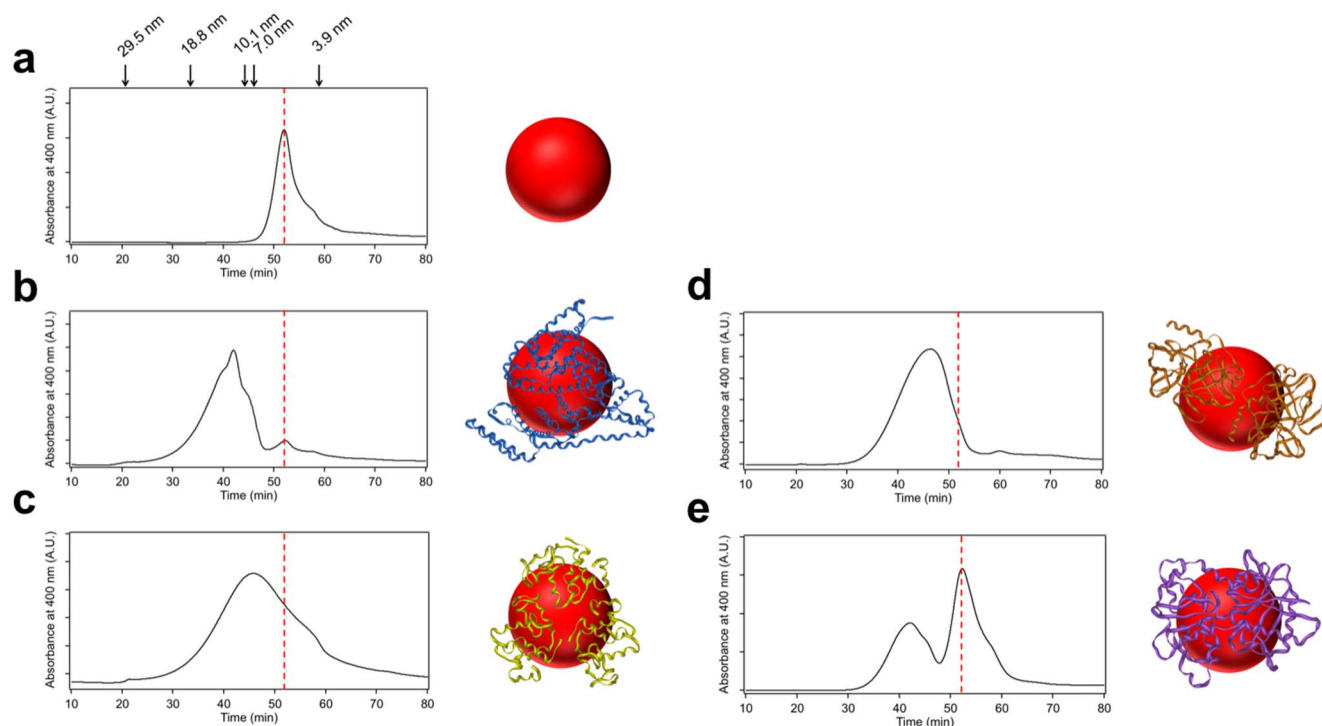


Figure 3 | Gel filtration chromatography of protein-functionalized QDs. (a) Unfunctionalized MPA-QDs. Hydrodynamic diameters of sizing standards are indicated above the graph (see Supporting Information Figure S2 for more details). (b) BSA-QDs. (c) Lysozyme-QDs. (d) Trypsin-QDs. (e) Transferrin-QDs. The red dashed line in each graph indicates the peak position of MPA-QDs.

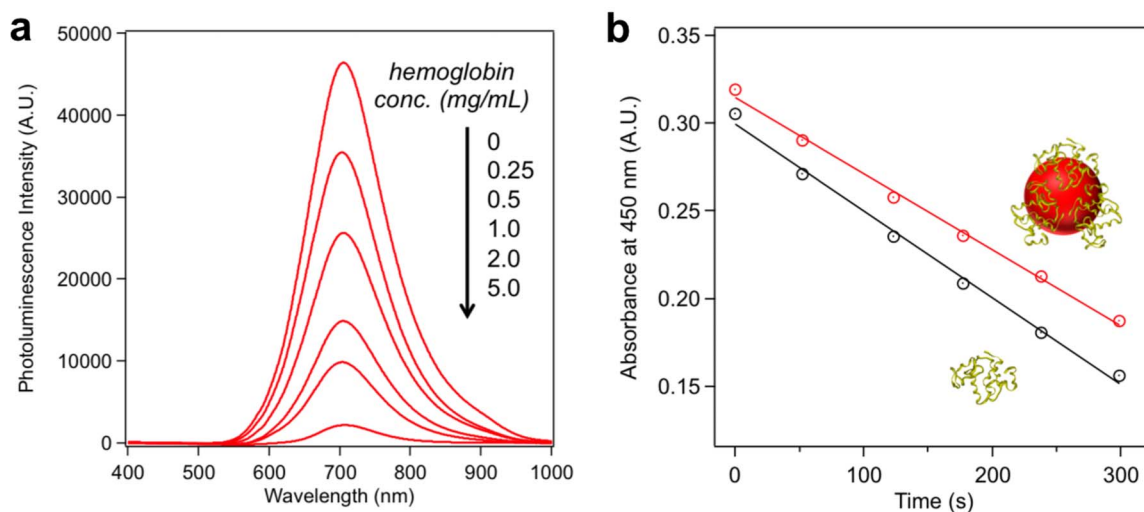


Figure 4 | Characterization of hemoglobin-QDs and lysozyme-QDs. (a) Photoluminescence quenching of $Zn_xHg_{1-x}Se$ QDs synthesized at different hemoglobin concentrations. (b) Determination of lysozyme activities in native form (black line) and QD-associated form (red line). Linear fit for native lysozyme: $y = -0.000495x + 0.299$; linear fit for QD-associated lysozyme: $y = -0.000434x + 0.315$. The slope is used to determine the lysis rate.

photobrightening effect with 54% and 51% increase of PL intensities respectively whereas the CdTe QDs were severely photobleached with 82% decrease of PL intensity (Figure 5a and SI section 3.3). The photobrightening effect of the as-prepared $Zn_xHg_{1-x}Se$ QDs is likely caused by the photo-annealing of the surface defects of the QDs. As a result, the QYs of the unfunctionalized and BSA-functionalized $Zn_xHg_{1-x}Se$ QDs increased to 42.5% and 41.0% after activation with the 405 nm laser for 1 hour. The photostability study was also performed on QDs films for $Zn_xHg_{1-x}Se$ QDs and CdSe QDs under continuous excitation with a 365 nm UV lamp (8 W). The CdSe QDs were quickly photobleached after 30 min excitation whereas the photoluminescence of $Zn_xHg_{1-x}Se$ QDs was retained even after 60 min excitation (SI section 3.3). The colloidal stability of BSA-functionalized $Zn_xHg_{1-x}Se$ QDs was evaluated at four different pHs (12.3, 9.0, 7.4, 5.2) during 20 days storage. Little fluctuation of QDs PL intensities, absorbance, and hydrodynamic sizes were observed for all the tested conditions, suggesting that the BSA-functionalized QDs possess robust colloidal stabilities (SI section 3.1). The non-specific cell imaging was conducted by incubating fixed HeLa cells with unfunctionalized MPA-QDs and the fluorescence images were captured on an inverted fluorescence microscope. As shown in Figure 5b, fixed HeLa cells can be readily stained with MPA-QDs showing a strong photoluminescence signal, suggesting that these $Zn_xHg_{1-x}Se$ QDs are well suited for cell imaging studies. When live HeLa cells were incubated with MPA-QDs no photoluminescence was detected (Figure 5b), indicating neglectable non-specific binding of MPA-QDs with live HeLa cells which most likely results from electrostatic repulsion between the negatively charged QDs and the negatively charged cell surface²⁷. Once the cell membrane is disrupted by cell fixation, the QDs can bind with the intracellular components of fixed cells non-specifically.

Specific cell imaging was explored using transferrin-functionalized $Zn_xHg_{1-x}Se$ QD as a probe. Transferrin can specifically bind with transferrin receptor on cell surface and is transported into the cell via receptor-mediated endocytosis²⁸. As shown in Figure 5b, transferrin receptor-expressing live HeLa cells incubated with transferrin-QDs exhibited strong photoluminescence signals, indicating high-level binding of transferrin-QDs with the cells. In contrast, no photoluminescence was detected for live HeLa cells incubated with BSA-QDs or MPA-QDs under the same conditions, implying that the cell binding of transferrin-QDs was specifically mediated by transferrin. The intracellular localization of transferrin-QDs is further investigated using confocal microscopy. As shown in Figure 5c, the transferrin-QDs were

internalized into HeLa cells and sequestered in small vesicles. There is a high co-localization between transferrin-QDs and lysotracker, implying that the QDs uptake is mediated by endocytic pathway.

Furthermore, this QD synthetic strategy could be extended to other biomolecules such as folic acid (FA) and peptide to produce biofunctionalized QDs (Figure 6a). Folic acid has been frequently used for cancer targeting since many cancer cells overexpress folic acid receptors²⁹. The FA-QDs were synthesized using FA and MPA molecules as co-ligands and the reaction condition is the same as protein-functionalized QDs (see experimental for details). The presence of FA molecules on QDs was confirmed using Fourier transform infrared spectroscopy (FTIR). The characteristic IR absorption peaks of FA molecules were detected for FA-QDs but not MPA-QDs (SI section 4.5). In addition, attachment of FA molecules to QDs leads to partial quenching of QD photoluminescence. As the FA concentration increases, more pronounced QD photoluminescence quenching is observed (SI section 4.6). This quenching effect has been previously observed and is attributed to the electron transfer between FA molecules and QDs³⁰. The FA-QDs exhibited robust colloidal stability at pH 7.4 over 7 days storage (SI section 3.2). Live HeLa cells incubated with FA-QDs exhibited strong photoluminescence (Figure 6b), indicating highly efficient cell binding of QDs mediated by FA molecules. Next, we selected a peptide (HHHHHHCGRK) to synthesize peptide-functionalized QDs. This peptide contains two domains including a cancer cell targeting domain (CGKRK) and a QD binding domain (HHHHHH). The tumor homing peptide CGKRK was initially identified using phage display and was found to specifically bind to MDA-MB-435 human breast cancer cell line³¹. The QD binding domain contains six histidine residues that are known to strongly coordinate with Zn^{2+} ions and have been utilized for QD bioconjugation¹³. The peptide-functionalized $Zn_xHg_{1-x}Se$ QDs were synthesized using the peptide and MPA molecules as co-ligands. The presence of peptide molecules on QDs was confirmed by agarose gel electrophoresis (SI section 4.1). Moreover, we found that the peptide itself (HHHHHHCGRK or HHHHHH) can mediate the growth of $Zn_xHg_{1-x}Se$ QDs in the absence of MPA molecules (SI section 2.3), suggesting that the QD synthesis and functionalization can be achieved in a single step. This is distinct from the previous study showing that the oligohistidine can be attached to the pre-synthesized QDs via histidine-zinc interaction¹⁶. As shown in Figure 6b, live MDA-MB-435S cells incubated with peptide QDs exhibited strong photoluminescence as a result of efficient QD binding. In contrast, no photoluminescence signal was

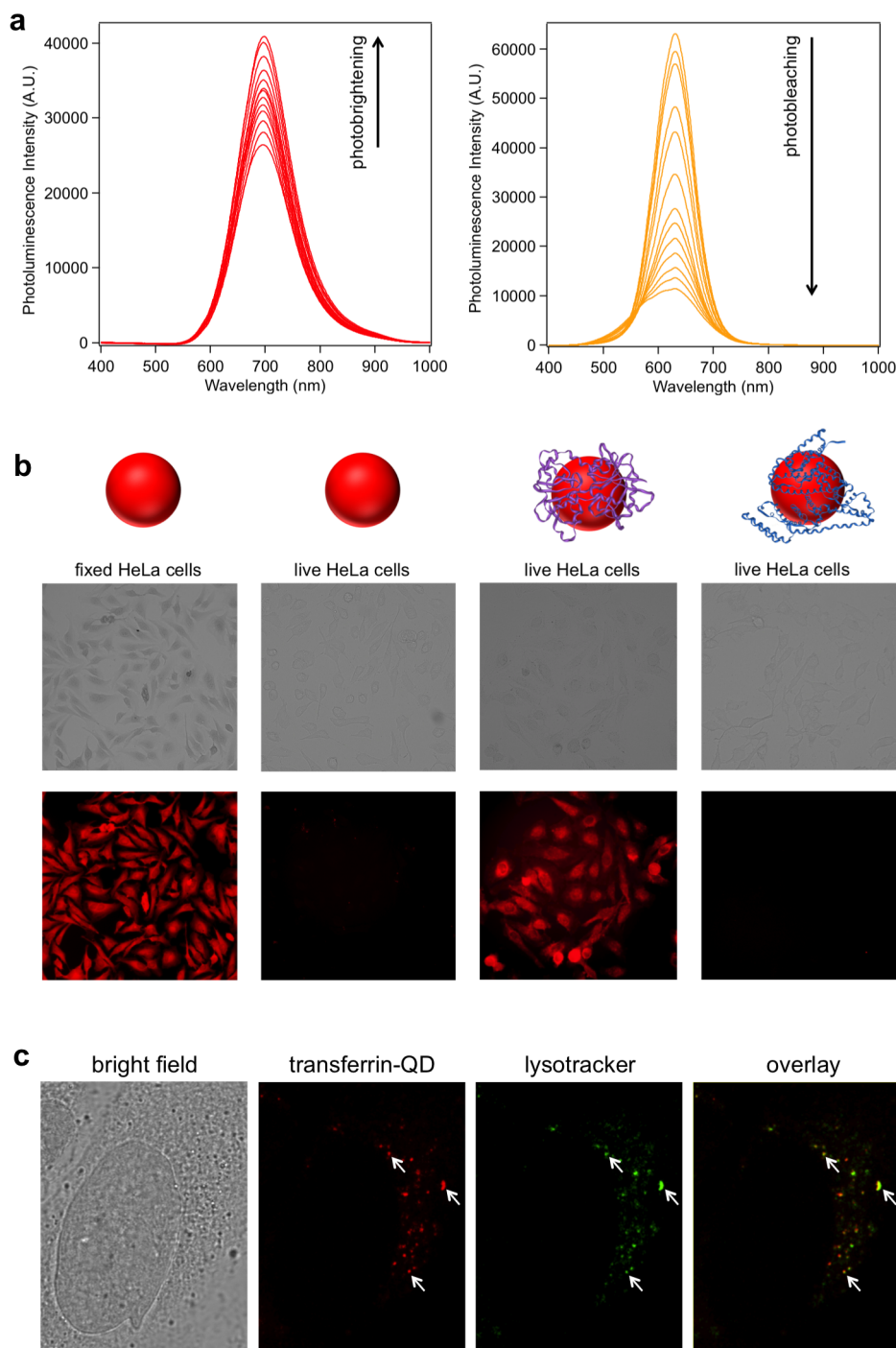


Figure 5 | $Zn_xHg_{1-x}Se$ QDs for cell imaging. (a) Photostability measurements of unfunctionalized $Zn_xHg_{1-x}Se$ QDs and CdTe QDs. Both QDs were continuously excited with a 405 nm laser (110 mW) and the photoluminescence spectra were recorded at different time points (0, 0.5, 1, 3, 5, 8, 12, 15, 20, 30, 40, 50, 60 min) (b) Bright field and fluorescence images of cells incubated with $Zn_xHg_{1-x}Se$ QDs. From left to right: fixed HeLa cells with MPA-QDs; live HeLa cells with MPA-QDs; live HeLa cells with transferrin-QDs; live HeLa cells with BSA-QDs. The images were acquired with a 10 \times objective. See Supplementary Information (section 4.5) for the fluorescence image acquired with a 40 \times objective which shows punctate patterns of cell staining. (c) Bright field and confocal fluorescence microscopy image of a single HeLa cell incubated with transferrin-QDs (red) and Lysotracker Green DND-26. The overlay image shows a high co-localization between the QDs and lysotracker. (Representative regions of overlap are indicated by arrows.)

detected for live MDA-MB-435S cells incubated with unfunctionalized MPA-QDs, suggesting that the cell binding of peptide-QD was specifically mediated by the peptide.

Discussion

We present a general facile strategy for one-step synthesis of biofunctionalized QDs. The reaction can be conducted in aqueous solution at

ambient conditions and completed within one second. The as-prepared biofunctionalized $Zn_xHg_{1-x}Se$ QDs exhibit strong photoluminescence, high photostability and can be used for specific cell targeting and imaging. The reported strategy to construct biofunctionalized QDs is much more straightforward than the traditional synthetic routes. We expect that this QDs synthesis strategy would be accessible to any laboratory that needs fluorescence labeling of biomolecules.

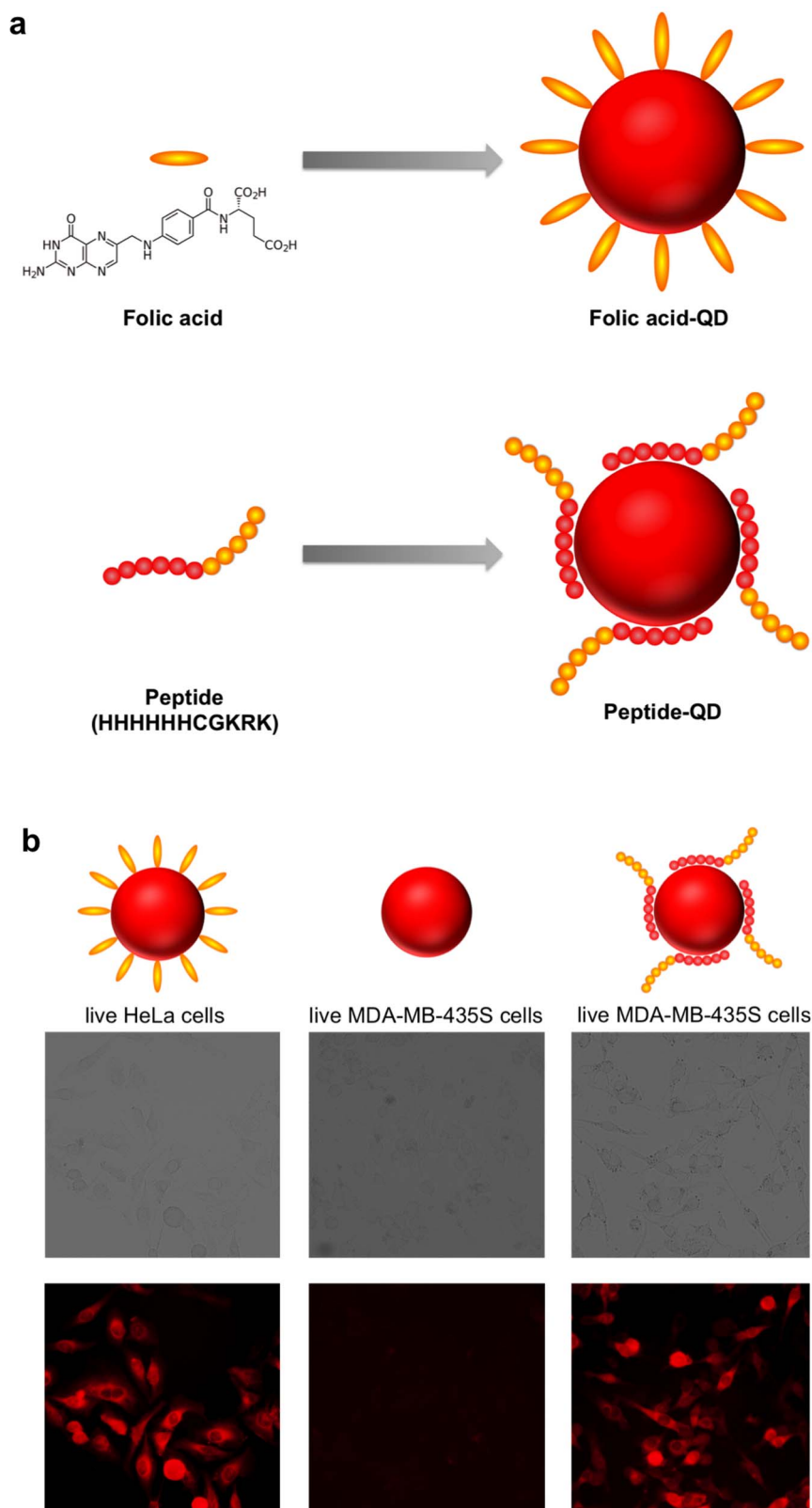


Figure 6 | Construction of folic acid- and peptide-functionalized $Zn_xHg_{1-x}Se$ QDs for cell imaging. (a) Schematic illustration of folic acid-QDs and peptide-QDs prepared in one-step synthesis. (b) Bright field and fluorescence images of cells incubated with $Zn_xHg_{1-x}Se$ QDs. From left to right: live HeLa cells with folic acid-QDs; live MDA-MB-435S cells with MPA-QDs; live MDA-MB-435S cells with peptide-QDs. The peptide sequence is HHHHHHCGRK. The images were acquired with a $10\times$ objective.

Methods

Materials. Zinc acetate dihydrate (99.0%), mercaptopropionic acid (MPA, 99%), selenium powder (99.99%), tellurium powder (99.997%), cadmium chloride (99.99%), sodium borohydride (98.0%), sodium selenite (98.0%), Coomassie brilliant

blue R-250 (dye content $\sim 50\%$, technical grade), albumin from bovine serum, hemoglobin from bovine blood, lysozyme from chicken egg white, TPCCK treated trypsin from bovine pancreas, transferrin from human, insulin, and *Micrococcus Lysodeikticus* were purchased from Sigma-Aldrich. Mercuric perchlorate (99.0%) was



purchased from Strem Chemicals. Ammonium hydrogen carbonate (NH_4HCO_3 , AR), sodium hydroxide (NaOH, AR), acetic acid (AR), hydrochloric acid (HCl, GR), nitric acid (HNO_3 , GR), bromophenol blue (AR), potassium bromide (AR) and folic acid (FA, BR) were purchased from Sinopharm Chemical Reagent Co., Ltd. Agarose powder was purchased from Biowest. Glycerol and tris(Hydroxymethyl) aminomethane (Tris) were purchased from Beijing Solarbio Science & Technology Co., Ltd. LysoTracker Green DND-26 was purchased from Invitrogen. Phosphate buffered saline ($10\times$ PBS) was purchased from Thermo Scientific (HyClone). Peptides (NH_2 -HHHHHHHCGRK-COOH and NH_2 -HHHHHHH-COOH, 98%) were purchased from ChinaPeptides Co., Ltd (Shanghai, China). HeLa cells were purchased from China Center for Type Culture Collection (CCTCC). MDA-MB-435S cells were purchased from Cell Resource Center of Shanghai Institutes for Biological Sciences, Chinese Academy of Sciences. Dulbecco's Modified Eagle's Medium (DMEM), fetal bovine serum (FBS), 0.25% trypsin/EDTA and phosphate buffered saline (PBS) were purchased from Hyclone. Leibovitz medium (L-15) was obtained from Gibco. Water used in all the studies was purified with a Milli-Q water purification system. All other reagents and solvents were of analytical grade.

Synthesis of unfunctionalized, protein-functionalized, folic acid-functionalized, and peptide-functionalized $\text{Zn}_x\text{Hg}_{1-x}\text{Se}$ QDs. Se precursor (250 mM NaHSe) was prepared by reducing 0.0197 g selenium powder with 0.0200 g sodium borohydride in 1 mL water at room temperature. The reaction was finished after complete dissolution of selenium powder to form a colorless solution.

To synthesize unfunctionalized $\text{Zn}_x\text{Hg}_{1-x}\text{Se}$ QDs, 125 μL $\text{Zn}(\text{OAc})_2$ (100 mM), desired volume (1.25, 2.5, 6.25, 12.5 or 25 μL) of $\text{Hg}(\text{ClO}_4)_2$ (100 mM), and 37.5 μL MPA (500 mM) were added to NH_4HCO_3 solution (0.2 M, pH = 12.3 adjusted by 10 M NaOH solution) to a total volume of 500 μL . Then 25 μL NaHSe (250 mM) was quickly injected into the precursor solution above followed by gently vortexing. The reaction solution turned brown immediately after adding NaHSe, indicating instant formation of $\text{Zn}_x\text{Hg}_{1-x}\text{Se}$ QDs.

To synthesize protein-functionalized $\text{Zn}_x\text{Hg}_{1-x}\text{Se}$ QDs, protein stock solution (100 mg/mL) was first prepared by dissolving protein powder (BSA, lysozyme, trypsin, hemoglobin, and transferrin) in $1\times$ PBS. For QD synthesis, desired amount of protein (final concentration: 0, 0.25, 0.5, 1.0, 2.0 or 5.0 mg/mL) was added together with 125 μL $\text{Zn}(\text{OAc})_2$ (100 mM), 12.5 μL $\text{Hg}(\text{ClO}_4)_2$ (100 mM), and 37.5 μL MPA (500 mM) to NH_4HCO_3 solution (0.2 M, pH = 12.3) to a total volume of 500 μL . Then 25 μL NaHSe (250 mM) was quickly injected into the precursor solution above followed by gently vortexing. The reaction solution turned to brown immediately after adding NaHSe, indicating instant formation of $\text{Zn}_x\text{Hg}_{1-x}\text{Se}$ QDs.

The synthesis protocol of folic acid and peptide-functionalized $\text{Zn}_x\text{Hg}_{1-x}\text{Se}$ QDs is same as protein-functionalized $\text{Zn}_x\text{Hg}_{1-x}\text{Se}$ QDs except that protein stock solution was replaced by folic acid stock solution and peptide stock solution, respectively. Folic acid stock solution (250 mM) was prepared by dissolving folic acid in NH_4HCO_3 solution (0.2 M, pH = 12.3). Peptide stock solution (100 mM) was prepared by dissolving the peptide (NH_2 -HHHHHHHCGRK-COOH) in H_2O . To synthesize folic acid-functionalized $\text{Zn}_x\text{Hg}_{1-x}\text{Se}$ QDs, 0, 2, 5, 10, 20, 50 μL folic acid stock solution were added for a 500 μL synthesis. To synthesize peptide-functionalized $\text{Zn}_x\text{Hg}_{1-x}\text{Se}$ QDs, 0, 15.5, 31.25, 62.5 μL peptide stock solution were added for a 500 μL synthesis.

Synthesis of CdTe QDs. Te precursor (NaHTe) was prepared by reducing 0.0400 g tellurium powder with 0.0250 g sodium borohydride in 1 mL water at 60°C for 40 minutes. To synthesize CdTe QDs, 6.25 μL CdCl_2 solution (100 mM in H_2O) and 1.25 μL MPA solution (500 mM in H_2O) were added to NH_4HCO_3 solution (0.2 M, pH = 8.5 adjusted by 10 M NaOH solution) to a total volume of 500 μL . Then 0.5 μL Te precursor was swiftly injected into the reaction mixture. The reaction was conducted at 100°C for 2 hours.

Optical characterization. QD samples were first purified via centrifugation at 6000 rpm for 3 min to remove any insoluble precipitation, and the supernatant QDs solution was collected for the measurements. The photoluminescence spectra were recorded using a fiber fluorescence spectrophotometer (AvaSpec-ULS2048-USB2) equipped with a 405 nm laser (110 mW) as excitation light source. The integration time was set to 20 ms. The absorption spectra were recorded using a UV-Vis spectrophotometer (Agilent 8453). Pure NH_4HCO_3 solution (0.2 M, pH = 12.3) was used as a blank for baseline correction.

QD elemental analysis. 50 μL $\text{Zn}_x\text{Hg}_{1-x}\text{Se}$ QD samples prepared with different Hg/Zn precursor ratios were first diluted to 500 μL with H_2O and then purified with MicrosepTM Advance Centrifugal Devices (YM-3, Pall Corporation) via centrifugation at 13500 rpm for 5 min to remove any free precursors. The purification was repeated twice. The purified QDs were recovered to 500 μL with H_2O and then digested with 1 mL concentrated HNO_3 at 90°C for 3 hours. The digested solution was diluted to 5 mL with H_2O . Quantitative elemental analysis of zinc, mercury, and selenium in each sample was performed on an inductively coupled plasma optical emission spectrometer (Varian 710-ES). A dilution series of zinc acetate, mercuric perchlorate, and sodium selenite solutions with known concentrations were made to generate standard curves.

TEM characterization. A few drops of each QD sample were dispersed onto a 3 mm copper grid covered with a continuous carbon film and were dried at room temperature. TEM characterization was performed using a JEOL JEM-2100

transmission electron microscope operating at 200 kV. STEM-EELS measurements were performed on a Tecnai G2 F20 S-Twin (FEI) transmission electron microscope.

Quantum yield determination. The QY is calculated according to the equation below:

$$\Phi_x = \Phi_{st} (I_x/I_{st}) (\eta_x^2/\eta_{st}^2) (A_{st}/A_x)$$

Where Φ is the quantum yield, I is the measured integrated emission intensity, η is the refractive index of the solvent, and A is the optical density. The subscript "st" refers to standard with known quantum yield and "x" refers to the QD sample. Fluorescence spectra were measured under 490 nm excitation. Rhodamine 6 G (QY = 95% in ethanol) was chosen as the standard.

Photostability measurements of $\text{Zn}_x\text{Hg}_{1-x}\text{Se}$ QDs, CdTe QDs, and CdSe QDs. Unfunctionalized $\text{Zn}_x\text{Hg}_{1-x}\text{Se}$ QDs, BSA-functionalized $\text{Zn}_x\text{Hg}_{1-x}\text{Se}$ QDs, and CdTe QDs ($\lambda_{em} = 630$ nm) were freshly prepared according to the protocol described above. QD samples were continuously excited with a 405 nm laser (110 mW) and the fluorescence spectra were recorded at different time points (0, 0.5, 1, 3, 5, 8, 12, 15, 20, 30, 40, 50, 60 min). Photostability studies were performed on QDs films for CdSe QDs and $\text{Zn}_x\text{Hg}_{1-x}\text{Se}$ QDs. The QD films were continuously excited with a 365 nm UV lamp (8 W) for 30 min and 60 min and the fluorescence images were recorded on an Olympus IX71 epifluorescence microscope with 1 millisecond acquisition time.

Colloidal stability measurements of $\text{Zn}_x\text{Hg}_{1-x}\text{Se}$ QDs. The pH of BSA-functionalized $\text{Zn}_x\text{Hg}_{1-x}\text{Se}$ QDs solution was adjusted with 0.1 M HCl to the desired value (12.3, 9.0, 7.4, 5.2) and then the QDs were stored at room temperature. The photoluminescence spectra, absorption spectra, and DLS data were recorded after 0, 1, 2, 3, 5, 7, 10, 15, 20 days. The pH of FA-QDs was adjusted to 7.4 with 0.1 M HCl and then the QDs were stored at room temperature. The photoluminescence spectra, absorption spectra, and DLS data were recorded after 0, 1, 3, 5, 7 days. Unfunctionalized $\text{Zn}_x\text{Hg}_{1-x}\text{Se}$ QDs were diluted 10 times in $1\times$ PBS and stored at room temperature. The photoluminescence spectra were recorded after 0, 1, 2, 3, 7, 10, 15, 20 days.

Agarose gel electrophoresis. 2 μL QD sample was mixed with 8 μL NH_4HCO_3 solution (0.2 M, pH = 12.3) and 2 μL $6\times$ agarose loading buffer and then loaded into 1% agarose gel. $1\times$ TA buffer (Tris/acetic acid) was used as the running buffer. The gel was run for 25 min at a constant voltage of 120 V and then imaged on a UV transilluminator of the UVP GelDoc-It 310 Imaging System with an excitation wavelength of 365 nm. The gel was subsequently stained with 0.1% Coomassie brilliant blue R-250 in 30% methanol and 10% acetic acid for 1 h and destained in 50% ethanol and 10% acetic acid for 24 h in an orbital shaker (TS-1, QILINBEIER) with the speed of 80 rpm before digital image acquisition.

Gel filtration chromatography. Gel filtration chromatography was performed using a SuperoseTM 6 10/300 GL column (GE Healthcare) conjugated to an Agilent 1260 Infinite HPLC system. Before running, each sample was purified via centrifugation at 10000 rpm for 5 min to remove any insoluble aggregates. The flow rate was fixed at 0.35 mL/min, the injection volume was 80 μL and each sample was run for an overall time of 80 min. The absorption wavelength used to monitor QDs was set at 400 nm. $1\times$ PBS (pH 7.4) was used as the running buffer. For nanocrystals sizing, a protein standards solution was prepared to include 15 μL blue dextran (25 mg/mL), 35 μL thyroglobulin (25 mg/mL), 15 μL alcohol dehydrogenase (25 mg/mL), 25 μL BSA (25 mg/mL), and 10 μL lysozyme (25 mg/mL).

Dynamic light scattering. Dynamic light scattering (DLS) measurements were performed on a Zetasizer Nano ZS90 (Malvern) with 90° scattering angle and a He-Ne laser.

Purification of $\text{Zn}_x\text{Hg}_{1-x}\text{Se}$ QDs. The QDs were first centrifuged at 10000 rpm for 5 min to remove any insoluble aggregates and then purified with a MicrosepTM Advance Centrifugal Devices (Pall Corporation) via centrifugation at 13500 rpm for 5 min to remove unreacted precursors and free ligand molecules. The selection of the molecular weight cut-off of the centrifugal device is dependent on the size of the ligands for QD synthesis. 3 kD cut-off filters are used to purify MPA-QDs, FA-QDs, and peptide-QDs; 30 kD cut-off filters are used to purify lysozyme-QDs; 100 kD cut-off filters are used to purify BSA-QDs and transferrin-QDs.

Circular dichroism spectrum. CD spectra of native BSA and QD-associated BSA were recorded on a circular dichroism spectrometer (Aviv Model-410, Biomedical). 3 mL of each sample was added into a 1 cm quartz cell and measured at the scan speed of 50 nm/min with a bandwidth of 2 nm. During the measurements the voltage of PMT detector of the CD spectrometer was maintained below 500 V.

Lysozyme activity measurements. The lysozyme activity was determined by the lysis rate of *Micrococcus lysodeikticus*. Lysozyme-capped $\text{Zn}_x\text{Hg}_{1-x}\text{Se}$ QDs were first purified with a MicrosepTM Advance Centrifugal Device (YM-30, Pall Corporation) via centrifugation at 13500 rpm for 5 min to remove free lysozyme. The purification step was repeated twice. The purified QDs were then recovered in $1\times$ PBS buffer to the initial volume. For each assay 0.05 mg *Micrococcus lysodeikticus* in 0.1 mL $1\times$ PBS was added into a flat transparent Corning 96-well plate, after which 0.1 mL native lysozyme (10 $\mu\text{g}/\text{mL}$) or lysozyme-capped QDs (lysozyme concentration



10 $\mu\text{g/mL}$) was added into the well containing *Micrococcus lysodeikticus* and quickly mixed. The absorbance of each sample at 450 nm was recorded using a multifunctional microplate reader (Tecan Infinite M200 Pro) every 60 seconds. The absorbance was plotted against the reaction time for the native lysozyme sample and the lysozyme-QD sample respectively. The ratio of the slopes for these two linear fits provides the percentage of remained lysozyme activity for the QD-associated lysozyme.

Fourier transform infrared spectroscopy (FTIR) characterization. Folic acid-functionalized $\text{Zn}_x\text{Hg}_{1-x}\text{Se}$ QDs were synthesized as described above. The QD sample was purified with a Microsep™ Advance Centrifugal Device (YM-3, Pall Corporation) via centrifugation at 13500 rpm for 5 min to remove free folic acid molecules, and the purification step was repeated twice. The purified QDs were then recovered in H_2O to the initial volume and then concentrated using a rotary evaporator (RE52CS-1, Shanghai Yarong) and dried in a hot oven (GZX-9030MBE, Shanghai Boxun). The QDs powder was mixed with potassium bromide 1 : 50 (w/w), grinded, and compressed into tablets. The infrared spectrum was recorded on a Fourier transform infrared spectrophotometer (Varian ProStar LC240). Folic acid and unfunctionalized QDs were used as controls.

Fixed cell imaging with unfunctionalized $\text{Zn}_x\text{Hg}_{1-x}\text{Se}$ QDs. HeLa cells were cultured on 25 cm^2 cell culture plates with vent caps (Corning) in DMEM supplemented with 10% fetal bovine serum in a humidified incubator at 37°C containing CO_2 (5%). HeLa cells that had been grown to subconfluence were dissociated from the surface with a solution of 0.25% trypsin/EDTA for 1 min. Then aliquots (500 μL , 5×10^4 cells) were seeded into a 24-well plate (Corning). After overnight incubation, the cells were fixed with 200 μL cold anhydrous methanol (stored at -20°C before experiment) for 15 min, then washed three times with PBS. The QDs were first purified with a Microsep™ Advance Centrifugal Device (YM-3, Pall Corporation) via centrifugation at 13000 rpm for 5 min and then recovered with NH_4HCO_3 solution (0.2 M, pH = 12.3) to the initial volume. The purified QDs were then diluted 1 : 2 with 1× PBS. The fixed HeLa cells were incubated with 120 μL diluted QDs for 30 min at room temperature and then washed twice with 1× PBS. The photoluminescence images were captured on an Olympus IX 71 inverted fluorescence microscope with 330–385 nm mercury lamp excitation and the QD emission signal was collected with a 420 nm long-pass filter.

Specific live cell imaging with transferrin, folic acid, and peptide-functionalized $\text{Zn}_x\text{Hg}_{1-x}\text{Se}$ QDs. HeLa cells were cultured and seeded as described above. MDA-MB-435 cells were cultured on 25 cm^2 cell culture plates with vent caps (Corning) in L-15 medium supplemented with 10% fetal bovine serum and 0.01 mg/mL insulin in a humidified incubator at 37°C. MDA-MB-435 cells that had been grown to subconfluence were dissociated from the surface with a solution of 0.25% trypsin/EDTA for 2 min. Then aliquots (500 μL , 5×10^4 cells) were seeded into a 24-well plate (Corning). After overnight incubation, the cells were washed once with 1× PBS. Transferrin, folic acid, and peptide-functionalized $\text{Zn}_x\text{Hg}_{1-x}\text{Se}$ QDs were first purified with a Microsep™ Advance Centrifugal Device (YM-3, Pall Corporation) via centrifugation at 13000 rpm for 5 min and then recovered with NH_4HCO_3 solution (0.2 M, pH = 12.3) to the initial volume. The purified QDs were then diluted 1 : 2 with 1× PBS and the pH was adjusted to 7 ~ 8 with diluted HCl. For transferrin and folic acid-functionalized QDs, HeLa cells were incubated with 120 μL diluted QDs at 37°C for 1 hour and then washed twice with 1× PBS. For peptide-functionalized QDs, MDA-MB-435 cells were incubated with 120 μL diluted QDs at 37°C for 1 hour and then washed twice with 1× PBS. Unfunctionalized QDs were used as a negative control for all the studies. The photoluminescence images were captured on an Olympus IX 71 inverted fluorescence microscope with 10× and 40× objectives with 330–385 nm mercury lamp excitation and the QD emission signal was collected with a 420 nm long-pass filter.

Confocal microscopy. Live cells were incubated with the QDs sample at 37°C for 1 h and washed twice with 1× PBS. After that the cells were incubated with 100 μL LysoTracker Green DND-26 solution (1 : 1000 diluted in serum-free cell culture medium) for 20 min and washed three times with 1× PBS. Confocal microscopy was performed on a Leica TCS SP5 II confocal laser scanning microscope using a 63× oil immersion objective. Localization of QDs was visualized with 405 nm diode laser excitation and the emission signal was collected between 650 and 750 nm. Localization of LysoTracker Green DND-26 was visualized with 476 nm argon laser excitation and the emission signal was collected between 500 nm and 600 nm.

- Alivisatos, A. P. Semiconductor clusters, nanocrystals, and quantum dots. *Science* **271**, 933–937 (1996).
- Bruchez Jr., M., Moronne, M., Gin, P., Weiss, S. & Alivisatos, A. P. Semiconductor nanocrystals as fluorescent biological labels. *Science* **281**, 2013–2016 (1998).
- Chan, W. C. W. & Nie, S. Quantum dot bioconjugates for ultrasensitive nonisotopic detection. *Science* **281**, 2016–2018 (1998).
- Michalet, X. *et al.* Quantum dots for live cells, in vivo imaging, and diagnostics. *Science* **307**, 538–544 (2005).
- Medintz, I. L., Uyeda, H. T., Goldman, E. R. & Mattoussi, H. Quantum dot bioconjugates for imaging, labeling and sensing. *Nature Mater.* **4**, 435–446 (2005).
- Kim, S. *et al.* Near-infrared fluorescent type II quantum dots for sentinel lymph node mapping. *Nat. Biotechnol.* **22**, 93–97 (2004).

- Jaiswal, J. K., Mattoussi, H., Mauro, J. M. & Simon, S. M. Long-term multiple color imaging of live cells using quantum dot bioconjugates. *Nat. Biotechnol.* **21**, 47–51 (2003).
- So, M.-K., Xu, C., Loening, A. M., Gambhir, S. S. & Rao, J. Self-illuminating quantum dot conjugates for in vivo imaging. *Nat. Biotechnol.* **24**, 339–343 (2006).
- Medintz, I. L. *et al.* Proteolytic activity monitored by fluorescence resonance energy transfer through quantum-dot-peptide conjugates. *Nature Mater.* **5**, 581–589 (2006).
- Resch-Genger, U., Grabolle, M., Cavaliere-Jaricot, S., Nitschke, R. & Nann, T. Quantum dots versus organic dyes as fluorescent labels. *Nature Methods* **5**, 763–775 (2008).
- Howarth, M. *et al.* Monovalent, reduced-size quantum dots for imaging receptors on living cells. *Nature Methods* **5**, 397–399 (2008).
- Choi, H. S. *et al.* Design considerations for tumour-targeted nanoparticles. *Nat. Nanotechnol.* **5**, 42–47 (2010).
- Medintz, I. L. *et al.* Self-assembled nanoscale biosensors based on quantum dot FRET donors. *Nat. Mater.* **2**, 630–638 (2003).
- Murray, C. B., Norris, D. J. & Bawendi, M. G. Synthesis and characterization of nearly monodisperse CdE (E = S, Se, Te) semiconductor nanocrystallites. *J. Am. Chem. Soc.* **115**, 8706–8715 (1993).
- Wu, X. *et al.* Immunofluorescent labeling of cancer marker Her2 and other cellular targets with semiconductor quantum dots. *Nat. Biotechnol.* **21**, 41–46 (2003).
- Liu, W. *et al.* Compact biocompatible quantum dots functionalized for cellular imaging. *J. Am. Chem. Soc.* **130**, 1274–1284 (2008).
- Ma, N., Marshall, A. F. & Rao, J. Near-infrared light emitting luciferase via biomineralization. *J. Am. Chem. Soc.* **132**, 6884–6885 (2010).
- Zhao, L. *et al.* Organophosphorus acid anhydrolase bio-template for the synthesis of CdS quantum dots. *Chem. Commun.* **47**, 7242–7244 (2011).
- Goswami, N. *et al.* Protein-directed synthesis of NIR-emitting, tunable HgS quantum dots and their applications in metal-ion sensing. *Small* **8**, 3175–3184 (2012).
- Ma, N., Sargent, E. H. & Kelley, S. O. Biotemplated nanostructures: directed assembly of electronic and optical materials using nanoscale complementarity. *J. Mater. Chem.* **18**, 954–964 (2008).
- Ma, N., Sargent, E. H. & Kelley, S. O. One-step DNA-programmed growth of luminescent and biofunctionalized nanocrystals. *Nat. Nanotechnol.* **4**, 121–125 (2009).
- Tikhomirov, G. *et al.* DNA-based programming of quantum dot valency, self-assembly and luminescence. *Nat. Nanotechnol.* **6**, 485–490 (2011).
- Peelle, B. R., Krauland, E. M., Wittrup, K. D. & Belcher, A. M. Design criteria for engineering inorganic material-specific peptides. *Langmuir* **21**, 6929–6933 (2005).
- Trzaskowski, B., Adamowicz, L. & Deymier, P. A. A theoretical study of zinc (II) interactions with amino acid models and peptide fragments. *J. Biol. Inorg. Chem.* **13**, 133–137 (2008).
- Smith, A. M. & Nie, S. Bright and compact alloyed quantum dots with broadly tunable near-infrared absorption and fluorescence spectra through mercury cation exchange. *J. Am. Chem. Soc.* **133**, 24–26 (2011).
- Janin, J. Surface and inside volumes in globular proteins. *Nature* **277**, 491–492 (1979).
- Grazu, V., Moros, M. & Sanchez-Espinel, C. *Nanobiotechnology: Inorganic Nanoparticles vs Organic Nanoparticles Ch. 14* (Elsevier, Oxford 2012).
- Hopkins, C. R. & Trowbridge, I. S. Internalization and processing of transferrin and the transferrin receptor in human carcinoma A431 cells. *J. Cell. Biol.* **97**, 508–521 (1983).
- Low, P. S., Henne, W. A. & Doorneweerd, D. D. Discovery and development of folic-acid-based receptor targeting for imaging and therapy of cancer and inflammatory diseases. *Acc. Chem. Res.* **41**, 120–129 (2008).
- Zhang, Y., Liu, J.-M. & Yan, X.-P. Self-assembly of folate onto polyethyleneimine-coated CdS/ZnS quantum dots for targeted turn-on fluorescence imaging of folate receptor overexpressed cancer cells. *Anal. Chem.* **85**, 228–234 (2013).
- Hoffman, J. A. *et al.* Progressive vascular changes in a transgenic mouse model of squamous cell carcinoma. *Cancer Cell* **4**, 383–391 (2003).

Acknowledgements

This work was supported in part by National Science Foundation of China (21175147), the Recruitment Program of Global Young Experts (1000-Young Talents Plan), the Project of Scientific and Technologic Infrastructure of Suzhou (SZS201207), the Priority Academic Program Development of Jiangsu Higher Education Institutions (PAPD), and startup funds from Soochow University.

Author contributions

X.H. and N.M. conceived and designed the experiments; X.H. and L.G. performed the experiments; X.H., L.G. and N.M. analyzed the data; N.M. wrote the manuscript.

Additional information

Supplementary information accompanies this paper at <http://www.nature.com/scientificreports>



Competing financial interests: The authors declare no competing financial interests.

How to cite this article: He, X., Gao, L. & Ma, N. One-Step Instant Synthesis of Protein-Conjugated Quantum Dots at Room Temperature. *Sci. Rep.* 3, 2825; DOI:10.1038/srep02825 (2013).



This work is licensed under a Creative Commons Attribution-NonCommercial-NoDerivs 3.0 Unported license. To view a copy of this license, visit <http://creativecommons.org/licenses/by-nc-nd/3.0>